Aluminum Wire Arc Additive Manufacturing Weld Parameters and Path Improvement

H. R. Peter*, K. M. Sargent*, ⸸T. Apairittirong, J. Penney*, and T. Schmitz*

*Department of Mechanical, Aerospace, and Biomedical Engineering, The University of Tennessee Knoxville, Knoxville, TN 37923

⸸Fronius USA LLC, Houston, TX 77064

Abstract:

Wire arc additive manufacturing (WAAM) is commonly used for low volume production and repair of metal parts in both commercial and defense applications due to its reduced time and cost compared to casting and forging. The selection of appropriate weld parameters is required to ensure fusion between beads, reduce porosity, and decrease defects. Additionally, path adjustments affect the heat distribution within each layer and the part dimensional accuracy. Gas metal arc welding (GMAW) tests were conducted with a KUKA KR 50 R2500 robot equipped with a Fronius welder to determine parameters for cold metal transfer (CMT) welding of 4943 aluminum. Using the CMT 1368 Adv (v1.2.0) synergic line, sufficient fusion between beads and weld quality was observed. Slicing programs were made in Rhinoceros7 and were used to modify the welding path so that dimensional inaccuracies from thermal gradients were reduced.

Introduction:

WAAM is a manufacturing process in which an electrical arc is used to weld metal wire to a substrate. Cross-sections of a three-dimensional (3D) computer model are deposited layer by layer to produce the near-net-shape part. Machining and heat treat operations are performed to achieve the final part geometry and properties. This process yields high deposition rates compared to most other metal additive manufacturing processes and is desirable in both defense and commercial low volume production applications for decreased time and cost compared to traditional casting, forging, and machining operations.

Cold metal transfer (CMT) is a welding method that utilizes shortage feedback to control wire feed resulting in reduced thermal effects on material properties, spatter, and deformation while demonstrating improved quality and consistency of welds [1]. While welding aluminum can be challenging due to its high electrical and thermal conductivities, deposition of aluminum alloys is relevant for their high strength-to-weight ratio and cost effectiveness. Aluminum alloys 4943, 4043, and 4047 are filler metals commonly used for WAAM [2], [3]. These alloys are often chosen for their weldability and corrosion resistance. While maintaining these

characteristics, the inclusion of magnesium in aluminum 4943 results in a higher as-printed strength [4].

The print path for aluminum WAAM strongly influences the deposited geometry. For example, changes in travel speed and direction may result in increased dwell time and, therefore, overbuilt volumes. In addition, the print path directly influences the temperature distribution throughout the part and results in either slower or faster solidification of the weld pool and associated residual stress and corresponding deformations.

Grasshopper is a parametric computer aided design (CAD) tool within the CAD modeling software Rhinoceros 7 [5]. Grasshopper scripts transform primitives such as points, curves, meshes, and coordinate frames into additive manufacturing tool paths. KUKA PRC is a plug-in for Grasshopper that enables programming of KUKA robot motion from a constructed series of frames, which are often discrete points along a curve and describe the desired path as time dependent joint angles that provide the desired end effector poses.

This paper demonstrates how common defects encountered during WAAM using CMT of aluminum 4943 were addressed through adjustments of the weld parameters, print path, and robot motion while considering their correlations. A series of prints with increasing complexity and requirements were conducted. The geometric inaccuracies were analyzed and solutions were tested.

Materials:

- Robotic arm - KUKA KR50 R2500
- Positioner - KUKA KP-2 HV 500
- Power supply – Fronius TPS CMT Advanced 4000
- FLIR A65 IR camera
- ZEISS ATOS-Q structured light scanner
- Aluminum 6061 203.2x203.2x12.7 mm substrate
- Aluminum ER 4943 1.2 mm diameter wire
- Gas supply - 100% Argon (40 cfm)

Figure 1: Hybrid cell: 6 DoF robot and 3 DoF positioner

Methods:

The robotic WAAM cell is displayed in Fig. 1. Part programs for this cell have previously been generated in Grasshopper from a poly-surface mesh of a constructed or imported CAD model in the Rhinoceros 7 virtual space. Grasshopper does this by slicing or separating the part mesh into layers along the vertical axis. It then applies contours and infill patterns in the form of curve primitives for each layer. All curves are discretized into a list of point primitives defined by Cartesian coordinate values, which are ordered to define the robot position sequence. Next, with each point defining an origin, frames are constructed and rotated to match desired welding tool orientations. The positioner (stacked rotary axes and linear rail) joint values are determined from frame positions and orientations for coordinated motion. Next, simulation and KUKA Robot Language (KRL) code are generated using the KUKA PRC plug-in.

While the previous KUKA PRC workflow enables complex, multi-axis printing, an alternative workflow is described here. It was developed to conveniently and quickly generate the programs for all prints in this research. This workflow incorporates Octopuz, a robot programming and simulation software, and demonstrates the flexibility offered by path construction using Rhinoceros 7. Within this alternative workflow, the list of Cartesian coordinates used to define the 3D pose of the robot's end effector was concatenated to match a

".path" file format with headers separating operations. The resulting ".path" file was imported into Octopuz where weld tool orientations and arc commands were applied.

Preliminary Testing

Because bead geometries are dependent on both torch velocity and wire feed rate, a preliminary test in which they were independently adjusted was conducted. In addition to bead geometry, feed rate and movement velocity dictate whether a weld can be completed due to the errors provided by the Fronius CMT Advanced 4000 if dwell time is too large or wire feed is prevented. Seven, two-layer beads were deposited with the parameters provided by Table 1.

Table 1 – Preliminary Test Movement Speeds and Wire Feed Rates

Bead Number	Movement Speed (mm/sec)	Wire Feed Rate (mm/sec)
1	143.33	9.90
2	143.33	9.90
3	148.33	9.90
4	150.00	9.90
5	150.00	11.00
6	150.00	13.00
7	150.00	11.00

While all beads deposited in this preliminary test applied the synergic description of "Standard Pulse," the test showed that continuous deposition free of errors is achievable for a velocity of 10 mm/s. This velocity was used for the following feed rate tests.

Test 1– First Layer Feed Rate

This test is meant to improve the weld quality and bead dimensions for the first layer deposited during a typical print by adjusting only one of the dependent variables. A different feed rate is required for the first layer from subsequent layers since the electrical penetration of and heat transfer to the 12.7 mm aluminum alloy 6061 plate is different from the electrical penetration and heat transfer for welding to a previous aluminum 4943 bead.

Six, 100 mm long beads were deposited with equal spacing of 30mm on a 203.2x203.2x12.7 mm aluminum 6061 plate at the best constant velocity from preliminary testing. Wire feed rate was increased with each bead by 0.33 mm/sec starting with 116.66 mm/sec and ending with 133.33 mm/sec. This range was chosen because previous experiences welding with this system suggested that 116.66 mm/sec would provide beads thinner than desired, while 133.33 mm/sec approaches the maximum feed rate allowed by the Fronius TPS 4000 for a CMT advanced synergic description.

Test 2 – Five Layer Feed Rate

Six, 100 mm single-bead walls were printed sequentially and with the same spacing of 30mm in Test 1. The first single bead layer was printed with the best feed rate determined from Test 1, since this should provide a good and consistent first layer to print over. After the first layer, four more layers with the same feed rate were deposited with a 30 second pause preceding. This pause allowed for a picture of the deposition to be taken, the temperature of the wall to be read, and cooling of the bead so that the preheated temperatures for the initial layers are too low while the preheated temperatures for the final layers are too high. The weld direction was alternated within each layer since alternating print direction helps mitigate temperature gradients caused by the current profile. Through comparison of the weld quality and dimensions to the preheated temperatures, an interpass temperature was established. The interpass temperature is the reference temperature used to determine when to start a new welding operation. This temperature ensures better welds, improved dimensional accuracy, and consistent layers throughout the build.

Test 3 – Stepover

Lack of fusion between adjacent beads can introduce significant porosity to the printed part. To ensure fusion between beads within the same layer, a sufficient stepover distance, the distance between parallel paths, is required. While a smaller stepover distance may improve the fusion between two parallel beads, significantly small stepover distances may result in vertical layering and rounded top surface.

Six pairs of walls were printed each with a stepover distance increasing by 1.5mm. The distances start at a minimum of 1.5 mm and end at a maximum of 9 mm. This range was chosen as preliminary testing suggested that these distances would capture both extreme cases of bead fusion. To replicate the temperature distribution experienced in a typical print, deposition of each pair was conducted layer by layer and weld direction was alternated with each layer. The build was cut perpendicular to the beads to reveal and assess the cross-section shown in Figure 10.

Test 4 – Spiral Path Blocks

Three infilled blocks with dimensions of 203.2x25.4x152.4 mm, 152.4x25.4x152.4 mm, and 152.4x25.4x152.4 mm were printed using the preferred parameters provided from the Preliminary Testing, Test 1 through Test 3, and a spiral path pattern with an offset starting location such as the path shown in Figure 2. Rectangular prisms with these dimensions were chosen to test the experimentally acquired welding parameters with a variety of length and width dimensions. A height of 152.4 mm (6.0 in.) was chosen as it was believed the number of layers required to meet this dimension would sufficiently test layer consistency. Lastly, the provided block dimensions allow samples with three differing orientations with respect to the CAD

reference frame to be machined from the blocks. These samples will be tested to determine the tensile strength of the as-printed part.

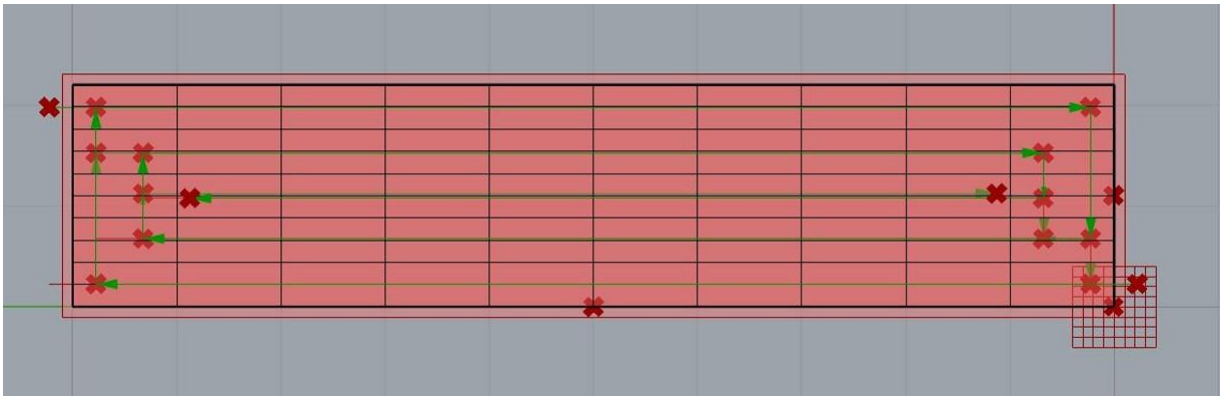

Figure 2 – Top View of Spiral Pattern for Block Printing from Rhinoceros 7

This spiral pattern was chosen as the printing strategy for these blocks to reduce the number of arc strikes and sharp corners which often cause inconsistent excess deposition. Starting location was alternated between one pair of opposing corners for every layer to mitigate excess material in the vertical axis at the ends of the block.

Measurement

All prints were scanned with the ATOS-Q GOM Structure Light Scanner, and meshes were polygonized within the software, Zeiss Inspect [6]. In this software, a series of ten lines were drawn perpendicular to the parallel bead paths for the scans of both Test 1 and Test 2, as shown in Figure 3 and Figure 4. Point cloud coordinate data gathered along eight of the ten lines was used to plot eight cross-sectional profiles. These profiles contained all six beads and were analyzed for height and width measurements, resulting in a width and height measurement for eight locations along each of the six beads. From the eight width and eight height measurements of each bead, an average bead width and average bead height were calculated. From these measurements, the standard deviation in width and height along each bead was also calculated (See Figure 12). Only the eight lines with distances of 10 mm to 80 mm were used to determine bead dimensions since the lines at 0 mm and 90 mm pass through the arc strike and crater locations, respectively, which have different dimensions based on dwell times and should not be included in the average bead width.

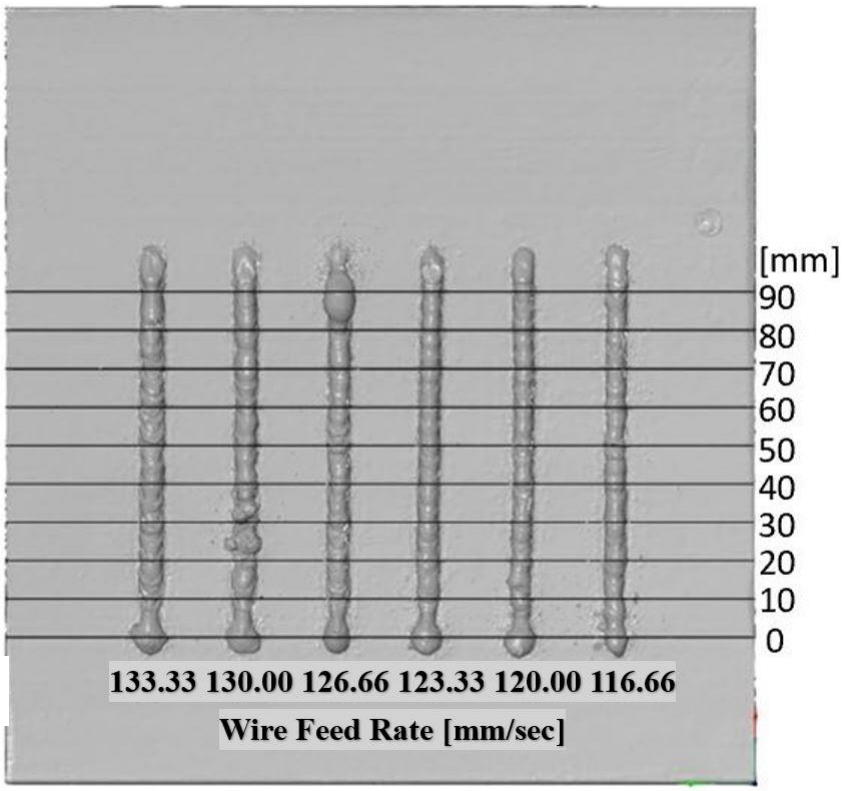

Figure 3 – First Layer Incremental Feed Rate Increase

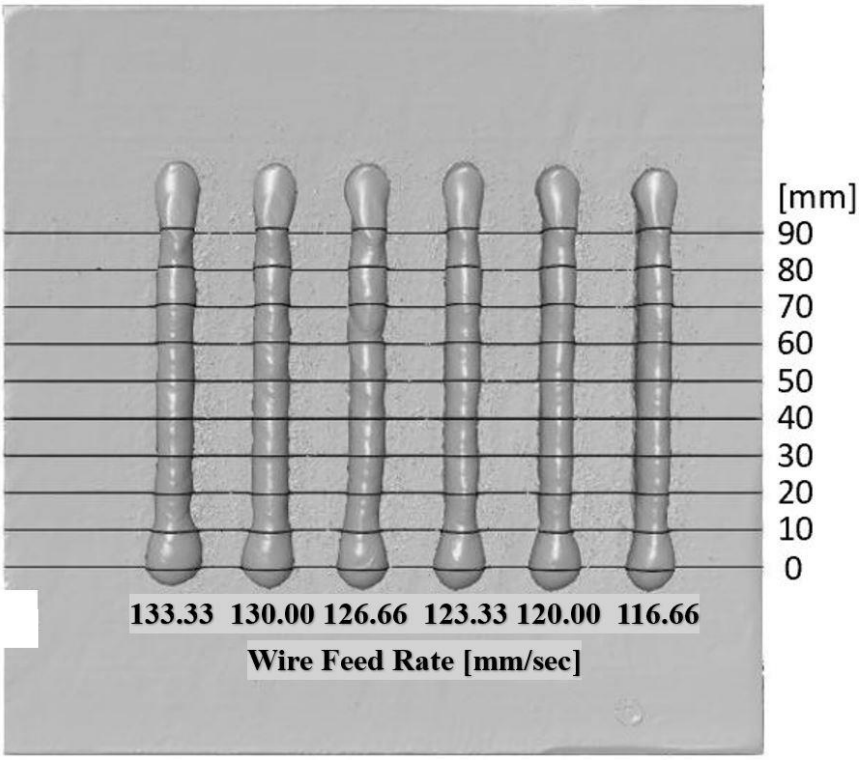

Figure 4 – Five Layers Incremental Feed Rate Increase

A heat map showing the surface deviation of the printed block from the CAD model was generated in Zeiss Inspect for one of the three blocks to quantify thickness of the excess material.

Results:

First Layer Test

From visual inspection of the one-layer bead depositions with varying wire feed rates, defects circled in Figure 5 were observed for feed rates of 126.66 and 130 mm/sec. Also observed were comparatively tall and narrow bead profiles for wire feed rates of 116.66, 120.00, and 123.33 mm/sec.

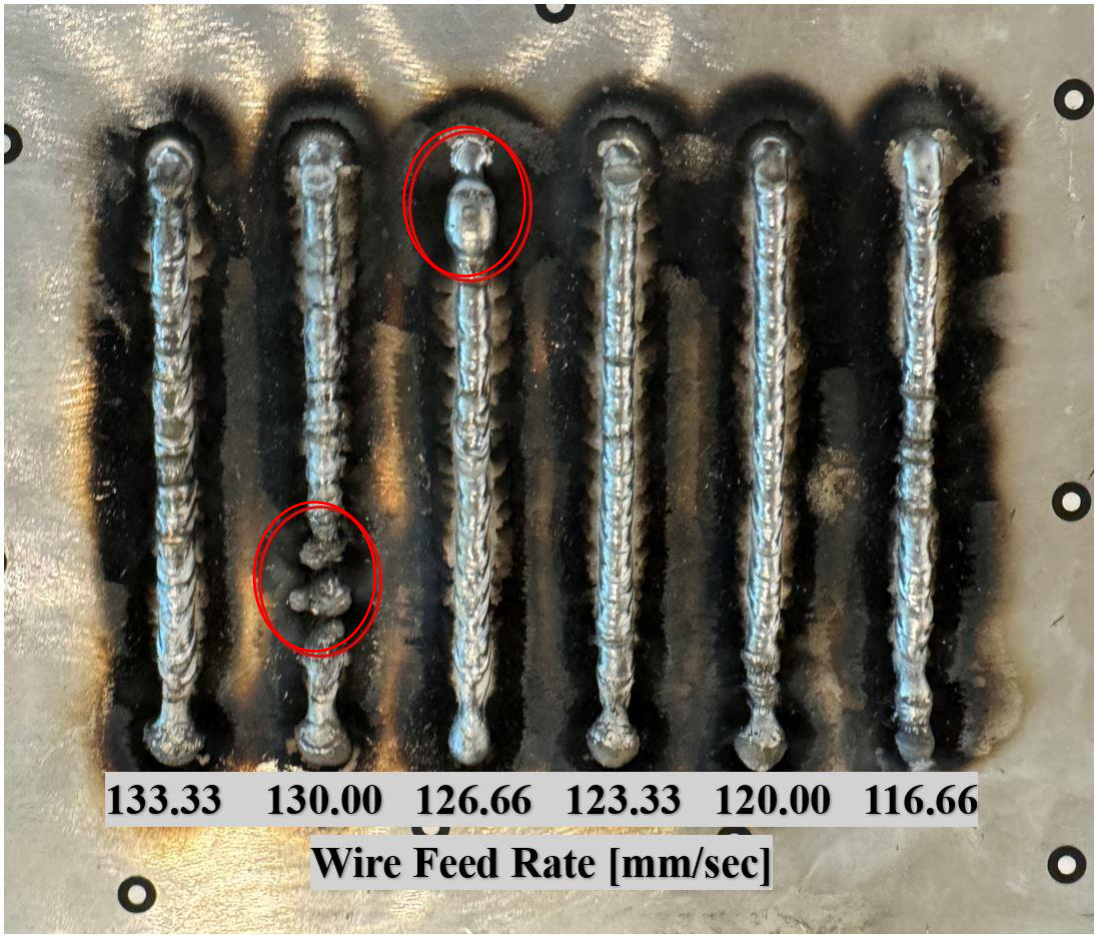

Figure 5 – First Layer Beads Deposited with Increasing Wire Feed Rate

Average bead dimensions and corresponding standard deviations as a function of wire feed rate shown in Figure 6 support the stated observations from the First Layer Test. In general, as wire feed rate increases, bead width increases and bead height decreases. Furthermore, for both plots a. and b. in Figure 5, the wire feed rate of 130.00 mm/sec exhibited the highest

standard deviation, which suggests this bead has the most inconsistent width and height measurements for the eight measurement locations. Large dimensional inconsistency along the 130.00 mm/sec feed rate bead is likely a result of the circled defect in Figure 5.

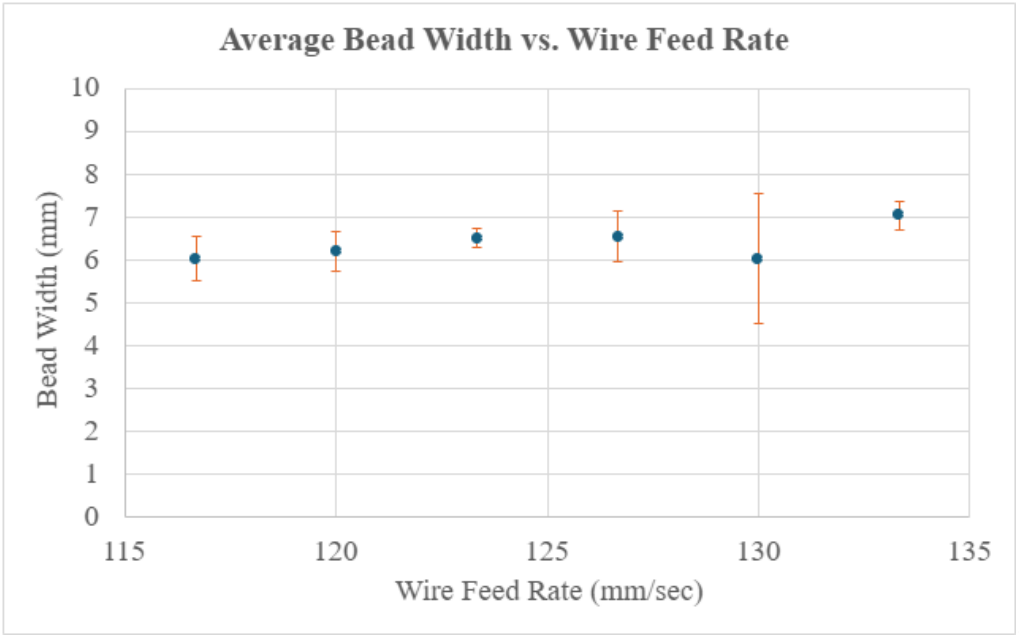

a.

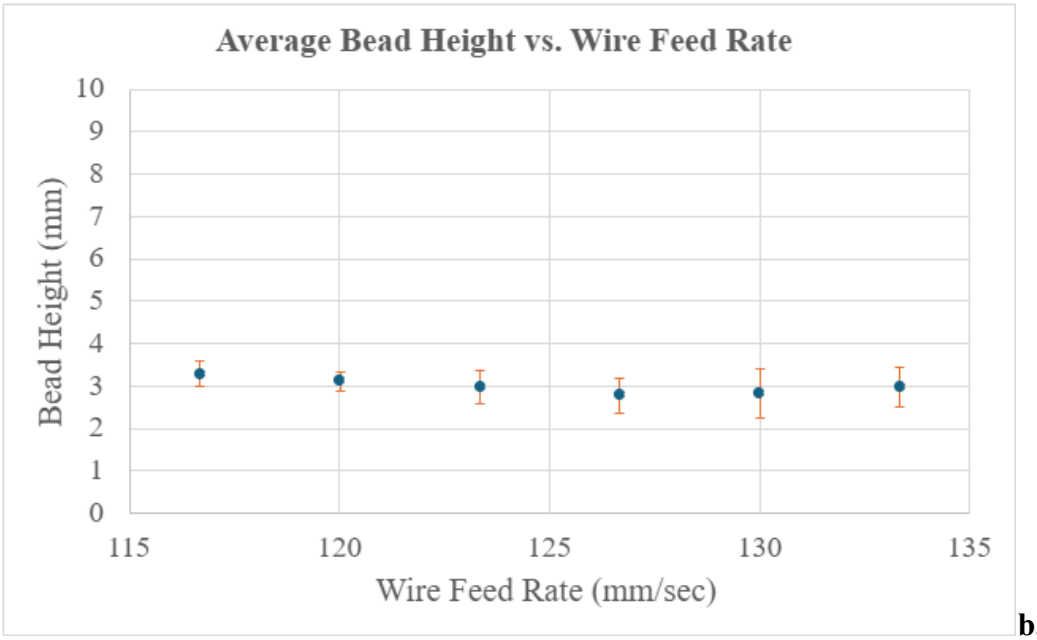

b.

Figure 6 – First Layer Average Bead Width and Height for Increasing Wire Feed Rate

Considering these observations and recognized trends in average bead dimensions, a wire feed rate of 133.33 mm/sec was selected as the desired feed rate since this feed rate produced the widest bead and should provide the most planar build. As will be discussed in the Block Test

section, planar build was an especially important consideration for the first layer, as preheating challenges resulted in significantly thin first layers.

Five Layer Feed Rate Test:

As can be seen in Figure 7, all walls deposited with varying wire feed rates were successfully built and show comparatively minimal large-scale defects. However, small porosities on the top surface were observed. Porosities such as the ones visible on the top surface of the walls in Figure 7, while undesirable, are likely caused by the higher preheat temperatures allowed to establish an interpass temperature.

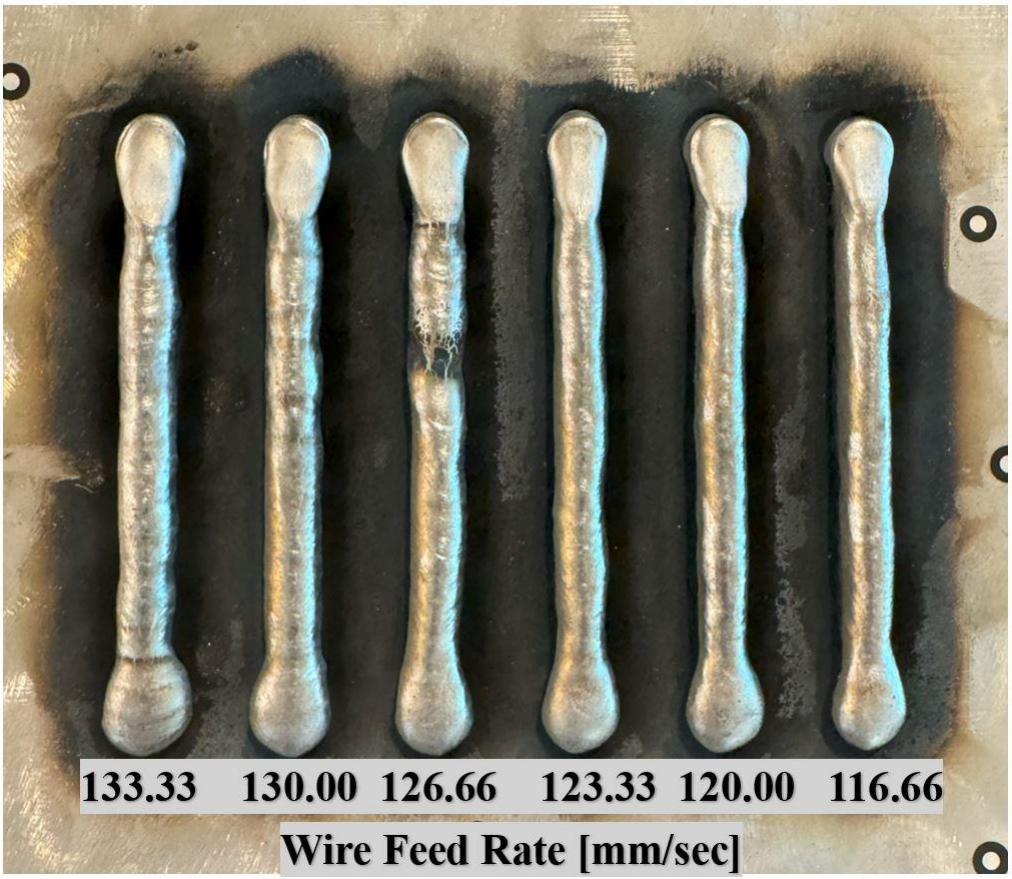

Figure 7 – Five Layer Test Walls Deposited with Increasing Wire Feed Rate

Similar to the First Layer Test, Figure 8 provides the average width and height dimensions measured at eight locations along each wall. The average wall width dimensions in Figure 8a show a slight increase for the middle two wire feed rates of 123.33 and 126.66 mm/sec, while the average height dimensions in Figure 8b display a slight decreasing trend with increasing wire feed rate. Relatively consistent standard deviations of around 1mm can be seen for both width and height dimensions.

In this case, increasing wall width was preferred over considering wall height, as excess material would allow large surface roughness to be machined away. For this reason, a wire feed rate of 125 mm/sec was selected for all subsequent layers.

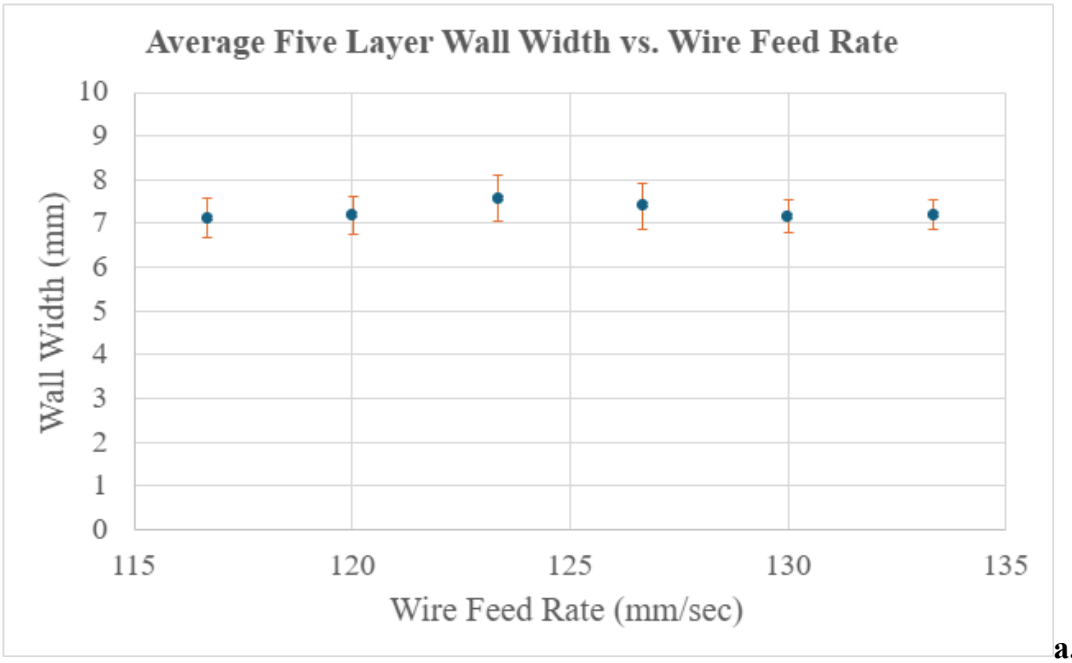

a.

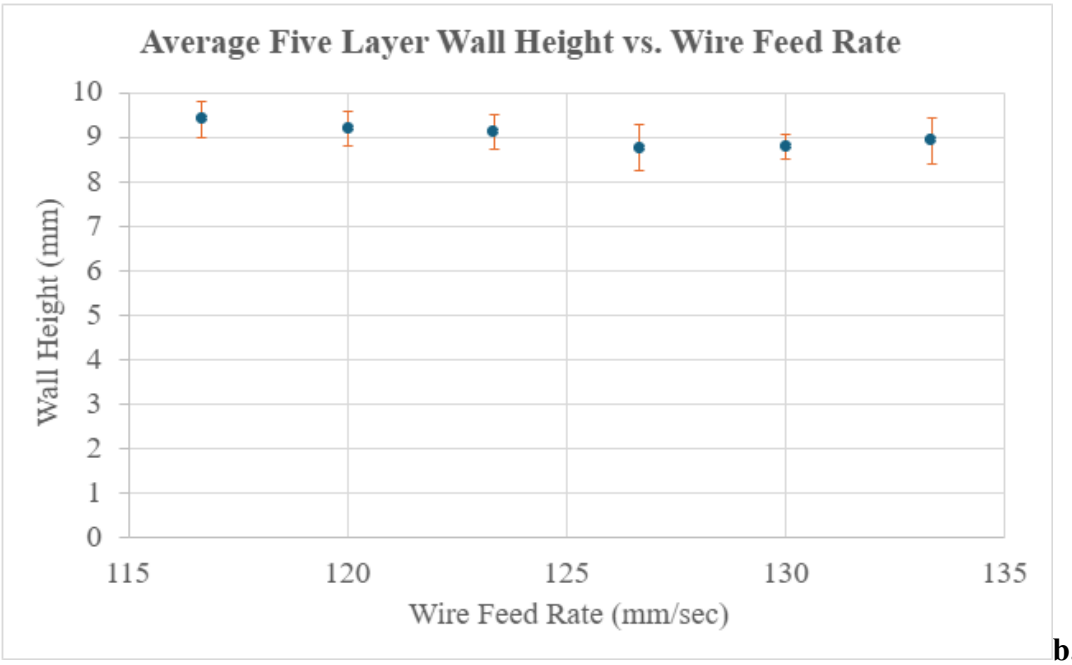

b.

Figure 8 – Average Five Layer Wall Width and Height for Increasing Wire Feed Rate

Of the images taken between each layer and corresponding measured pre-heat temperatures, 56℃ provided the best layered bead with no porosity visible from the outside. For these reasons, 56℃ was chosen as the interpass temperature.

Stepover Test

Figure 9 provides a top view of the six deposited bead pairs with increasing stepover distance from right to left. This view provided an initial understanding of fusion for the six stepover distances. From this view, a lack of fusion was observed for stepover distances of 6, 7.5, and 9 mm while pairs with stepover distances of 1.5, 3.0, and 4.5 mm appeared to be fully fused.

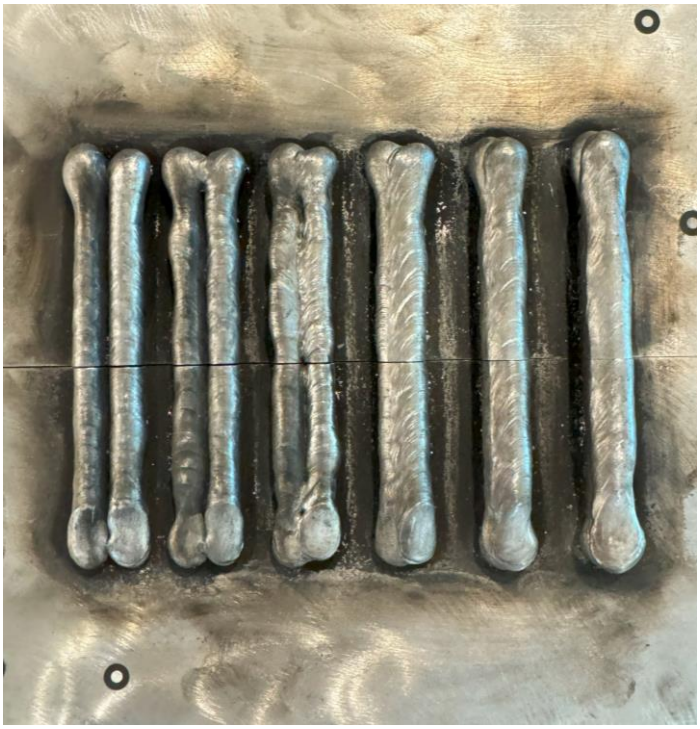

Figure 9 – Top View of Fusion Test Depositions

Results expressed in Table 2 from inspection of the build cross-section shown in Figure 10 agree with observations from the top-view inspection. Additionally, a second peak could not be distinguished for pairs with stepover distances less than 4.5 mm, which suggests significant overlap with and remelting of the first deposition. Based on these results, 4.5mm was selected for the stepover distance of future tests since complete fusion between depositions and a flatter top surface was observed for this distance.

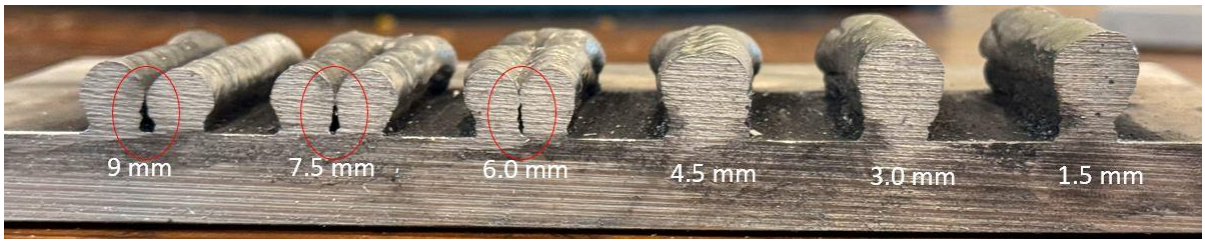

Figure 10 - Stepover Build Cross-Section and Indicated Lack of Fusion

Table 2 – Fusion Assessment of Deposition Pairs with Increasing Stepover Distance

Step Over Distance (mm)	Lack of Fusion (Yes/No)
1.5	**No**
3	**No**
4.5	**No**
6	**Yes**
7.5	**Yes**
9	**Yes**

Block Test

Shown in Figure 11 are two views of each of the three printed test blocks. For all three blocks, sagging along each edge, significant planar build at all four corners, and noticeably thinner initial layers can be seen. Preheating to a temperature of roughly 56℃ when printing the first block provided the narrow first few layers, which can be seen at the bottom of the block in Figure 11e. As a result, an interpass temperature of 56℃ was determined to be too cold for blocks of these dimensions. Printing was initiated at incrementally higher preheat temperatures until a preheat temperature of 95℃ was reached and sufficient bead width was observed. In this test, a blow torch was used to preheat the plate before printing each block, however, this method was insufficient for large blocks, and preheat temperatures above 60℃ proved considerably challenging to achieve. This resulted in cold and narrow layers until welding provided enough heat to reach the 95℃ interpass temperature. Overall deformation appears to be consistent between the 203.2x25.4x152.4 mm and 152.4x25.4x152.4 mm blocks. However, outlined in Figure 11e. is a significant indentation absent in the other two blocks. During this print, obstacles

presented by the welding torch prevented print initiation at the interpass temperature, which could not be achieved again. The colder preheat temperature resulted in a narrow layer and the indentation outlined.

Figure 11 – Front and Isotropic Views of Three Spiral Path Test Blocks

Measurement of surface deviation of the 203.2x25.4x152.4 mm block from the CAD model in Zeiss Inspect provided the heat map and various labeled points of interest shown in Figure 12. This deviation map indicates a relatively constant surface deviation of roughly positive 4 mm along the longest side. As suggested from visual inspection, the vertical edges have greater planar build with deviation around positive 6 to 7 mm. While still providing excess material, initial layers show surface deviation less than 0.5mm.

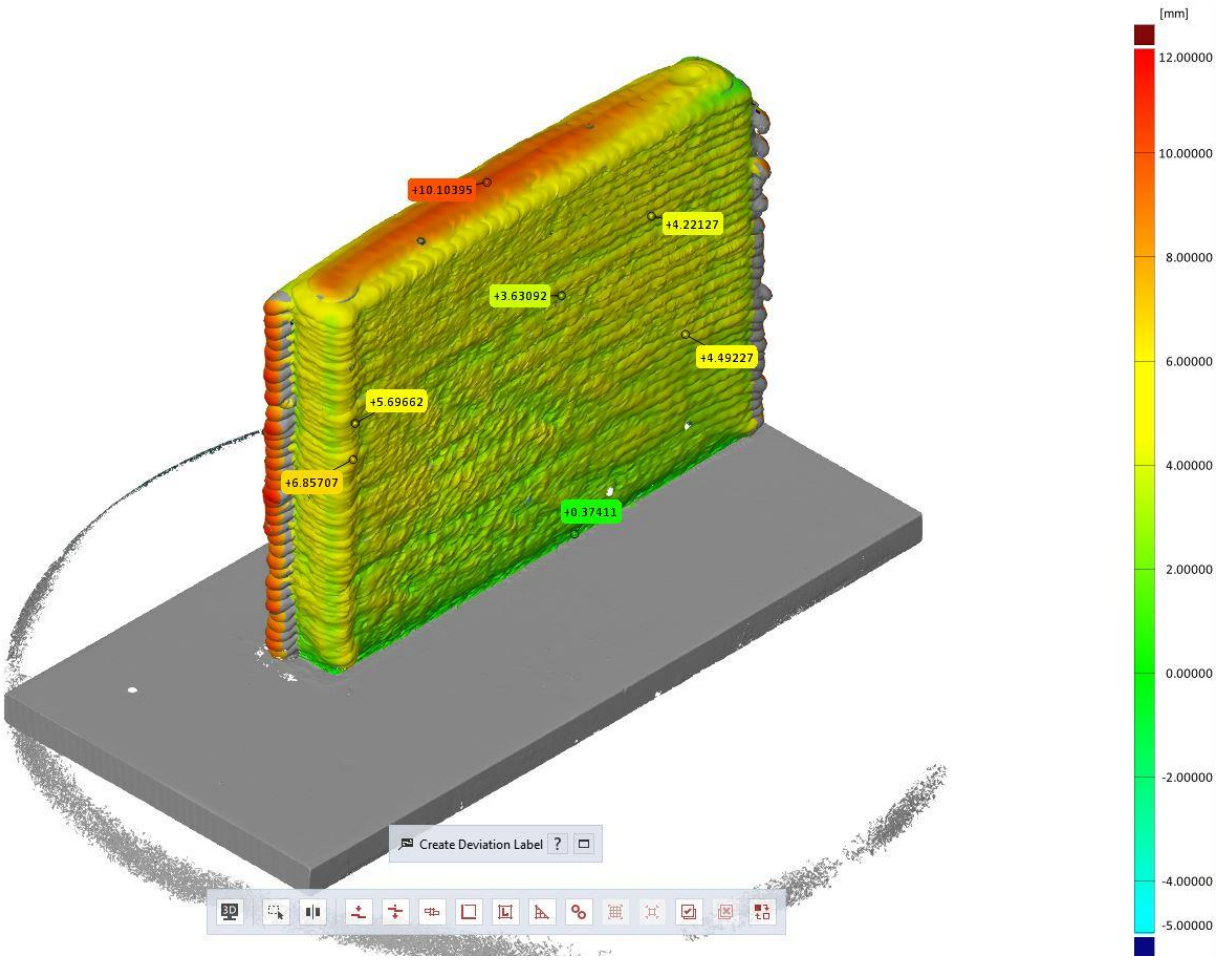

Figure 12 – Surface Deviation of 203.2x25.4x152.4 mm WAAM Block from CAD

Table 3 summarizes required materials and experimentally determined welding parameters from all four tests. “Thin Contour Interpass Temp” refers to the interpass temperature necessary for prints that are 1 to 2 beads thick, while “Thick Part Interpass Temp" refers to parts thicker than 2 beads.

Table 3 – Summary of Welding Parameters

Layer Number	Welding wire	Diameter (mm)	Gas	Wire feed speed (mm/sec)	Traveling speed (mm/sec)	Thick Part Interpass temp °C	Thin Contour Interpass temp °C	Layer Height (mm)	Stepover (mm)
1	ER4943	1.2	Ar 100%	133.33	10	85-95	56	2.2	4.5
2+	ER4943	1.2	Ar 100%	116.66	10	85-95	56	2.2	4.5

Conclusion:

The reduced time, reduced cost, and high complexity offered by WAAM compared to casting in low volume production combined with the superior as-printed strength to many other filler metals were the primary motivations for this research. In combination with welding parameters, the parametric tool Grasshopper in Rhinoceros 7 provides close control over welding paths crucial to achieving desired geometries and mitigating defects. The Grasshopper scripts and workflows developed for this research can be used in further research exploring the relationship between weld path, temperature, geometry, and material properties. While this research addresses CMT GMAW of aluminum alloy 4943, further testing is required for WAAM through other welding methods. Furthermore, the concluded parameters provided in Table 3 were determined with consideration for geometry. Currently, research is being conducted to reduce the large deviations from planar build at sharp corners and sagging of top edges. More work is being conducted to determine and improve as-printed material properties resulting from these parameters.

References:

[1] "CMT - cold metal transfer: the cold welding process for premium quality," Fronius, https://www.fronius.com/en-us/usa/welding-technology/world-of-welding/fronius-welding-processes/cmt

[2] N. Coniglio, C. E. Cross, I. Dörfel, and W. Österle, "Phase formation in 6060/4043 Aluminum Weld Solidification," *Materials Science and Engineering*, vol. 517, no. 1–2, pp. 321–327, Aug. 2009. doi:10.1016/j.msea.2009.03.087

[3] A. S. Haselhuhn, P. G. Sanders, and J. M. Pearce, "Hypoeutectic aluminum–silicon alloy development for GMAW-based 3-D printing using Wedge Castings," *International Journal of Metalcasting*, vol. 11, no. 4, pp. 843–856, Jan. 2017. doi:10.1007/s40962-017-0133-z

[4] B. Anderson, T. Anderson, G. White, and P. B. Patrick, "New Development in Aluminum Welding Wire - Alloy 4943," presented at the SNAME Maritime Convention, Providence, RI, USA, Oct. 2012. https://doi.org/10.5957/SMC-2012-P16

[5] "Kuka: PRC - parametric robot control for grasshopper," Food4Rhino, https://www.food4rhino.com/en/app/kukaprc-parametric-robot-control-grasshopper

[6] "ZEISS INSPECT - the metrology software for all challenges," ZEISS, https://www.zeiss.com/metrology/en/software/zeiss-inspect.html